Volume 315, number 2, 119–124 FEBS 11940 January 1993

Low pH crystal structure of glycosylated lignin peroxidase from *Phanerochaete chrysosporium* at 2.5 Å resolution

Klaus Piontek, Tuomo Glumoff and Kaspar Winterhalter

Laboratorium für Biochemie I, Eidgenössische Technische Hochschule Zürich, Universitätstr. 16, CH-8092 Zürich, Switzerland

Received 6 November 1992

The heme-containing glycoprotein lignin peroxidase (pI 4.15) has been crystallized at pH 4.0. The structure of the peroxidase from the orthorhombic crystals has been determined by multiple isomorphous replacement. The model comprises all 343 amino acids, one heme molecule, and three sugar residues. It has been refined to an *R*-factor of 20.3%. The chain fold of residues 15 to 275 is in general similar to those of cytochrome *c* peroxidase. Despite binding of the heme to the same region and a similar arrangement of the proximal and distal histidine as in cytochrome *c* peroxidase a significantly larger distance of the iron ion to the proximal histidine is observed. Distinct electron density extending from Asn-257 and at the distal side of the heme indicates ordered sugar residues in the crystal.

Crystal structure; Lignin degradation; White-rot fungus; Peroxidase; Heme protein; Glycoprotein

1. INTRODUCTION

The basidiomycetous white-rot fungus *Phanerochaete chrysosporium* is capable of degrading lignin, the structural part of wood, through its lignin degrading enzymes. Lignin is an essential component of woody tissues providing rigidity to vascular plants. Structurally, lignin is a complex three-dimensional biopolymer made up of oxygenated phenylpropane units linked together primarily with the β-O-4 bond, but also with various other C–C and C–O linkages [1]. Two extracellular heme peroxidases, lignin peroxidase (or ligninase) and manganese dependent peroxidase are secreted by the fungus when an essential nutrient, such as carbon or nitrogen is depleted [2]. Leisola et al. [3] determined up to 15 heme proteins in the extracellular fluid of ligninolytic cultures of *P. chrysosporium*.

Lignin peroxidase is a 40 kDa, monomeric, glycosylated enzyme that exhibits an unusually low pH-optimum [4]. It contains one Fe protoporphyrin IX molecule and exists as multiple isozymes. Together with other enzymes it is thought to constitute the major components of the lignin degradative system of *P. chrysosporium*, although its exact role in vivo is under debate [5]. It catalyzes a H_2O_2-dependent oxidative reaction of non-phenolic electron-rich aromatic compounds. Like other heme peroxidases, such as horseradish peroxidase and cytochrome *c* peroxidase, lignin peroxidases exhibit typical reactions [6] (for an overview on heme proteins see [7]). On the other hand lignin peroxidases are unique in one respect, namely the ability to oxidize compounds of high redox potential such as lignin and its model compounds ([8] and references therein) and a variety of xenobiotics [9].

Based on analogous kinetic and spectral properties of LIP with CcP the three-dimensional structures are presumably similar; but this had not been proven. We determined the structure of LIP415 and present the first tertiary structure of a lignin peroxidase.

Correspondence address: K. Piontek, Laboratorium für Biochemie I, Eidgenössische Technische Hochschule Zürich, Universitätstrasse 16, CH-8092 Zürich, Switzerland. Fax: (41) (1) 261 5677.

**Present address:* Turku Centre for Biotechnology, Tykistökatu 6, BioCity, SF-20520 Turku, Finland.

Abbreviations: LIP, lignin peroxidase; LIP415, lignin peroxidase isozyme with pI 4.15; CcP, cytochrome *c* peroxidase; m.i.r., multiple isomorphous replacement; r.m.s., root mean square.

2. EXPERIMENTAL

2.1. *Enzyme purification, crystallization and crystal properties*

Lignin peroxidase was produced and purified as described earlier [10]. Absorption spectra of the protein showed maxima at 635, 502 and 408 nm, typical for normal ferric heme [11]. Crystals were grown at room temperature using the hanging drop method [12]. 5 μl samples containing 12 mg/ml protein were mixed with 5 μl 30% saturated ammonium sulfate, buffered to pH 4.0 with 100 mM sodium citrate, and vapor equilibrated against 1 ml of the same solution. Seeding techniques with macroseeds [13] were essential to obtain large single crystals. With this procedure single crystals grow routinely to dimensions of $0.8 \times 0.5 \times 0.3$ mm^3. Ligninase crystals belong to the space group $P2_12_12_1$ with unit cell dimensions a = 61.27 Å; b = 74.91 Å; c = 106.40 Å. With one monomeric molecule per asymmetric unit, a V_m value of 2.92 Å^3/Da is calculated according to Matthews [14]. The crystals diffract to at least 1.8 Å and are very stable in X-rays. Even after an exposure of more than 24 hours the crystals still diffract to high resolution.

2.2. *Data collection and processing*

Diffraction intensities of the native and three isomorphous heavy atom derivative crystals were collected on the Siemens/Nicolet X-100A

Table I

Data collection and processing statistics of native and heavy atom crystals

	Native	K_2PtCl_4	K_2PdCl_4	K_2HgI_4
Number of crystals used	1	1	1	2
Soaking conditions (mM)		3	5	0.5
(days)		2.5	3	6
Resolution (Å)	2.0	2.2	2.2	2.5
Measured reflections	95521	59790	59257	72792
Unique reflections	31261	19953	21266	17009
Completeness (%)[1]	79.0	73.7	78.9	94.1
R_{merge} (%)[2]	6.8	8.0	8.3	10.3
R_{scale} to native (%)[3]		20.8	12.0	11.7
Number of sites		4	3	1

[1] The native data are 88.1% complete up to 3.0 Å resolution.

[2] $R_{merge} = (\Sigma_h |(< I_h > - I_h)| / \Sigma_h I_h) \times 100$

where $< I_h >$ is the mean of the I_h observations of reflection h.

[3] $R_{scale} = (\Sigma_h |(FH_h - F_h)| / \Sigma_h |0.5 \times (FH_h + F_h)|) \times 100$

Where FH_h and F_h stands for the structure factor amplitudes of reflection h of the heavy atom derivative and native data respectively.

area detector of the EMBL-Heidelberg, Germany. An Elliott GX-18 rotating anode with monochromatized CuK_α radiation has been employed. The crystals were mounted b* along the spindle axis and oscillated for 0.25° per frame. Processing was performed using the program XDS [15]. Intensity measurements were merged and scaled by programs of the Groningen BIOMOL crystallographic software package. The results are summarized in Table I.

2.3. *Structure determination and refinement*

In an effort to solve the structure using the molecular replacement method with the refined model of CcP [16] two different programs for the rotation function problem were employed. One was the Crowther rotation function [17] within the program package MERLOT [18] and the other one was the reciprocal rotation function based on the algorithm of Rossmann [19]. Despite several rotation function calculations with various parameters and resolution shells no convincing solution was achieved.

Therefore m.i.r. was attempted. Numerous commonly used heavy atom compounds [12] were screened for their ability to form derivatives with the enzyme. The native crystals were soaked in mother liquor supplemented with the heavy atom compounds and intensity changes were monitored by recording precession pictures of the principal zones. K_2PtCl_4, K_2PdCl_4, and K_2HgI_4 proved to be useful derivatives for analysis to higher resolution (Table II).

Originally only the data of the native, the Pd- and Pt-derivative crystals were available. The major site of the Pd-derivative was readily interpreted from difference Patterson maps. Based on only this site, phases were calculated which were used to reveal other sites in the Pt-derivative and to assign the two derivatives to the same origin in the space group $P2_12_12_1$. Cross-phasing by means of difference Fourier maps was done to make sure that no false peak in the Patterson maps was interpreted as heavy atom site. The initial m.i.r.-map based only on the Pd- and Pt-derivative phases had a mean figure of merit of 0.62 for data up to 3.0 Å. This map was not interpretable in terms of the polypeptide chain. Solvent flattening [20] including phase extention from 5.0 to 3.0 Å, assuming a maximum solvent content of 50 percent, improved the quality of the electron density significantly. The overall figure of merit increased to 0.82. The heme molecule with the proximal and distal histidine could immediately be recognized as a prominent feature in the resulting electron density maps. From then on about 60 percent of the polypeptide chain, almost exclusively the helical regions, could be assigned to its electron density. The availability of the third derivative data set gave an additionally improved m.i.r.-map which

Table II

Refinement of heavy atom parameters

		x	*y*	*z*	occ.	*B*	Ph.	R_c	*R*
K_2PtCl_4	1	0.521	0.256	0.169	4.49	117.2			
	2	0.425	0.109	0.025	2.86	50.8			
	3	0.103	0.838	0.031	2.40	26.7			
	4	0.163	0.125	0.156	1.82	2.6	2.70	0.55 (891)	9.37
K_2PdCl_4	1	0.184	0.132	0.221	1.83	−3.7			
	2	0.897	0.388	0.076	1.06	19.8			
	3	0.238	0.170	0.179	1.26	41.5	1.33	0.81 (1126)	7.96
HgI_4	Hg	0.214	0.142	0.009	2.48	30.2			
	I1	0.183	0.130	−0.009	1.06	−25.3			
	I2	0.245	0.169	0.004	0.80	−28.9			
	I3	0.195	0.150	0.032	1.30	−28.3	4.44	0.52 (1161)	4.01

x, *y*, *z*, fractional coordinates; occ., relative occupancy; *B*, temperature factor; Ph, phasing power: r.m.s. heavy-atom F/r.m.s. lack of closure; R_c, Cullis *R*-factor.

Number of reflections included in brackets.

$R_c = (\Sigma \| F_{PH} \pm F_p| - F_{H(calc)}| / \Sigma |F_{PH} - F_p|) \times 100$; *R*, *R*-factor: $R = (\Sigma |F_{PH(obs)} - F_{PH(calc)}| / \Sigma F_{PH(obs)}) \times 100$

Figure of merit (FOM) as a function of resolution of the combined m.i.r. phases

Res. (Å)	11.71	8.28	6.40	5.22	4.40	3.81	3.36	3.00	Total	19-3 Å
FOM	0.81	0.87	0.84	0.83	0.77	0.73	0.67	0.62	0.71	

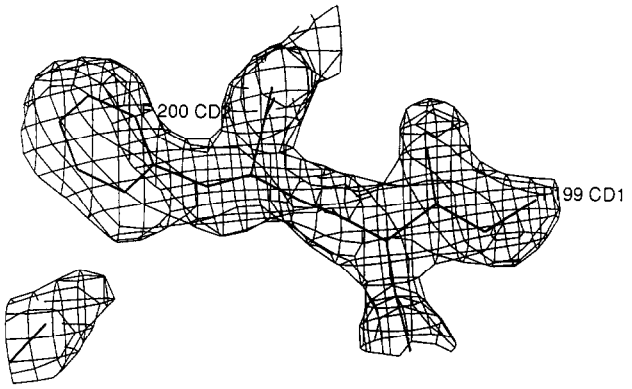

Fig. 1. Example of the final electron density map ($(2|F_o| - |F_c|)\alpha_c$) of residues Ile-199 and Phe-200.

was of such a quality (Table II) that it allowed us to build a total of about 80 percent of the amino acids and the heme molecule. Only residues 308 to 343 in the C-terminal region and residues 214 to 223 in a loop region could not be identified at this point. Based on these coordinates an *R*-factor of 43.1% for 6.0 to 3.0 Å resolution data was calculated.

All calculations were done utilizing programs of the CCP4 suite. Model building was performed with the programs FRODO [21] and 'O' [22] implemented on an Evans and Sutherland PS340 picture system and on a Silicon Graphics 4D/220 GTX, respectively.

Refinement of the model proceeded with the programs XPLOR [23] and PROLSQ [24]. Five rounds of molecular dynamics with simulated annealing and refinement cycles and successive model building were performed. Two rounds with 6.0 to 3.0 Å resolution data and three rounds with data up to 2.5 Å resolution were done. The remaining residues could be assigned to difference electron density maps after the first round of refinement with the 2.5 Å data. The heme group was restrained to an ideal geometry obeying perfect planar quadratic conformation of the pyrrole rings with the iron atom 1.96 Å away from the nitrogens. The iron to proximal histidine distance was not restrained. An additional four cycles of conventional restrained least squares refinement utilizing the program PROLSQ were done within the same resolution shell. No restraints were put then on the linkage of the metal atom to the nitrogens of the pyrrole rings and the planarity of the heme group. The final overall *R*-factor is 20.3% for all the observed 14301 reflections between 6.0 and 2.5 Å resolution. The current model comprises all 343 amino acids, the heme molecule, and three sugar residues. The sugar molecules were not included in the refinement. No solvent structure has been built yet. The model has good geometry with r.m.s. deviations from ideal geometry of 0.02 Å and 1.5° for bond lengths and angles, respectively. Individual temperature factor refinement was included at this stage. The average *B*-factor is 12.6 Å^2.

A complete description of the structure solution and the refined atomic model of LIP415 will be published elsewhere.

3. RESULTS AND DISCUSSION

The final electron density maps based on the phases from the atomic positions enabled us to place all amino acids of the polypeptide chain and the heme molecule unambiguously. An example of the final $2F_o-F_c$ map is shown in Fig. 1. The amino acid sequence deduced from the cDNA clone L18 encoding LiP2 was reported [25]. This sequence was used for model building of the polypeptide and showed the best agreement with the electron density.

The fold of lignin peroxidase is mostly helical (Fig. 2) and the enzyme is divided into two domains. Each domain is essentially located on either side of the heme plane. The C-terminal portion (residues 276 to 343), which is unique to the lignin peroxidase if compared to C*c*P, forms a mostly extended chain with little contact to the rest of the protein. Only three separate single turns of a 3_{10}-helix and a short piece of β-strand (comprising only two residues) are found in this region (Fig.

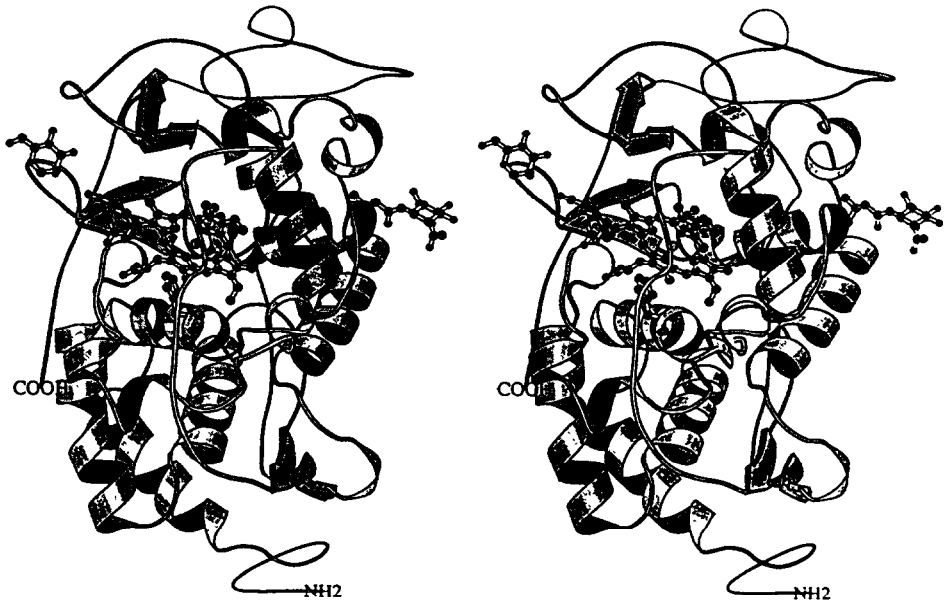

Fig. 2. Ribbon sketch of lignin peroxidase in stereo. The heme molecule with the proximal and distal histidine, one *N*-acetylglucosamine molecule (upper right portion of the plot), and two mannose molecules (upper left part of the picture) at the active site entrance are also shown. The diagram was drawn by the program package MOLSCRIPT [31].

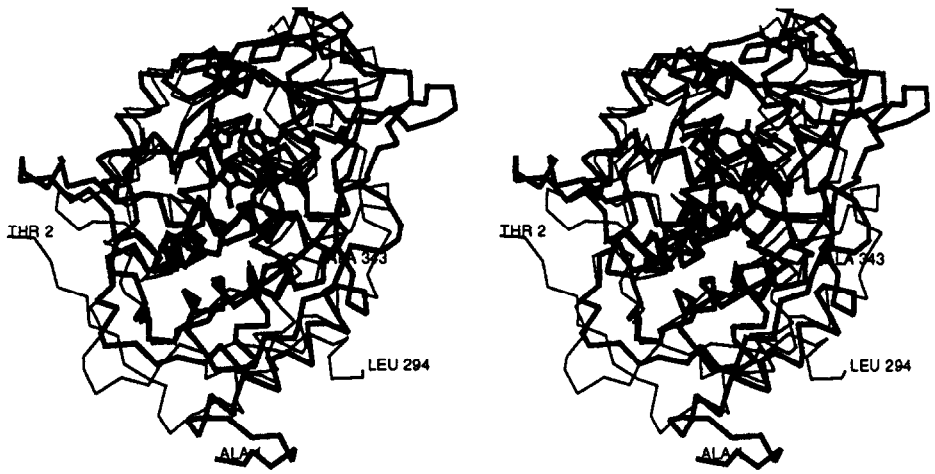

Fig. 3. C_α stereo-plot of LIP415 (thick lines, residues 1 to 343) superimposed with C*c*P (thin lines, residues 2 to 294). For the sake of clarity only the heme group of the lignin peroxidase structure is shown in addition.

2). It connects the two domains and folds in part across the active site entrance.

All eight cysteine residues in LIP415 form disulfide bridges and give the protein a high degree of rigidity which is reflected in a relatively low overall temperature factor. One disulfide bridge formed by residues 317 and 249 is located in the C-terminal peptide. Despite low sequence homology with C*c*P and the fact that this enzyme does not form one single disulfide bridge the folds are in general similar. The C_α-atoms of residues 15 to 275 of C*c*P can be superimposed on the LIP415 structure with an overall r.m.s. of 1.8 Å (Fig. 3).

The sequence Asn-X-Ser/Thr, typical for an *N*-glycosylation site, exists once in LIP415 for residues 257–259. Schmidt et al. [26] found for several lignin peroxidase isozymes that there are two *N*-acetylglucosamines and 14 to 18 mannose residues. They also propose that these enzymes are also *O*-glycosylated because the enzyme deglycosylated by Endo H still stained strongly with a glycoprotein-specific stain. We found discrete density extending from the imido nitrogen of Asn-257 into the solvent region. Fig. 4 shows one *N*-acetylglucosamine built into an electron density map which was calculated with model phases from which the sugar molecule has been omitted.

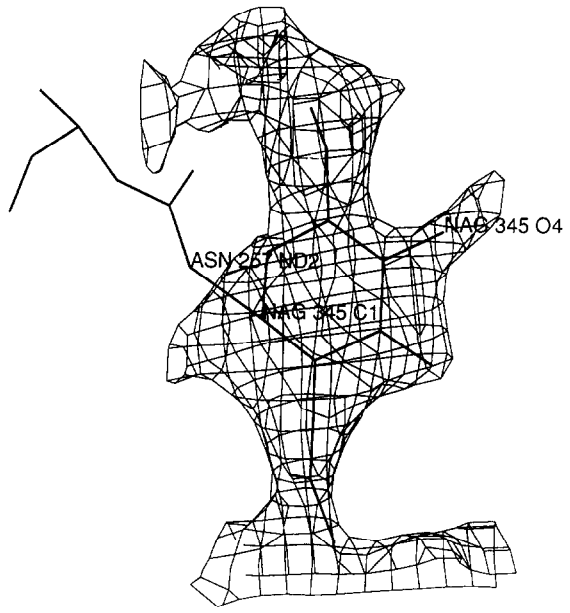

Fig. 4. Electron density map ($(|F_o| - |F_c|)\alpha_c$) of the *N*-acetylglucosamine (NAG) molecule bound to Asn-257. The contribution of the sugar molecule for the phase calculations was omitted.

There are a total of 41 Ser/Thr residues which are potential sites for *O*-glycosylation. Eleven Ser/Thr residues are clustered within the C-terminal peptide. It is most probable that this region contains *O*-glycosylation site(s) in agreement with discrete electron density extending into the solvent region from the hydroxyl groups of two threonine residues.

The heme molecule binding and the arrangement of the proximal and distal histidine resembles C*c*P. But there are significant differences. The distance of Nε2 of the proximal histidine to the iron atom is 2.28 Å which is substantially larger than usually found in heme proteins [27]. In C*c*P [16] this distance is only 1.96 Å. The difference of roughly 0.3 Å is probably not significant from a statistical point of view since it is close to the positional error of the atoms at the present 2.5 Å resolution. On the other hand there are structural features in the ligninase molecule which reveal chemical reasons for the longer Fe–N distance. The proximal histidine 176 is situated in a 3_{10}-helix which is formed by residues 173 to 178. This portion of the polypeptide chain has moved away up to about 1.0 Å from the heme plane (Fig. 5) if compared with the situation in C*c*P. Responsible for this displacement seems to be Ser-177. Its hydroxyl group is within hydrogen bonding distance to the mainchain O and N and sidechain OD2 of Asp-201.

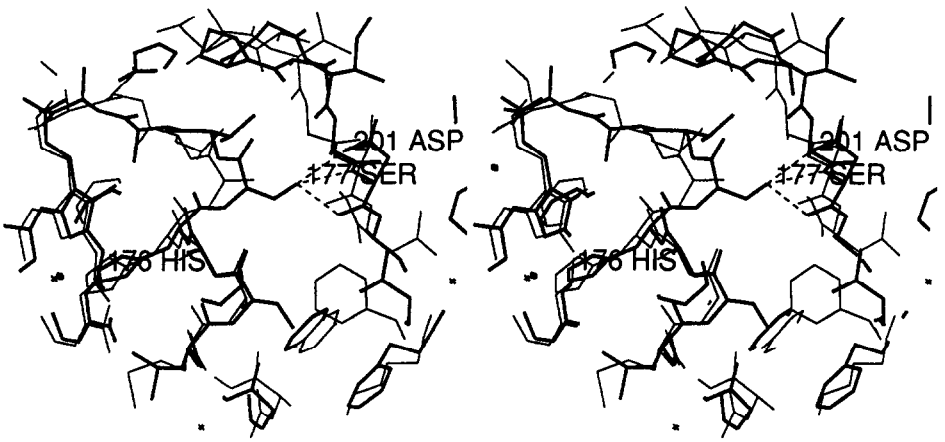

Fig. 5. Stereo-plot of LIP415 (thick lines) superimposed with CcP. Shown is the proximal histidine containing helix and its vicinity. Hydrogen bonds are in dashed lines.

Especially the hydrogen bond formed with the carbonyl oxygen is very strong as judged by a 2.5 Å distance. Cytochrome *c* peroxidase is not able to build up such a hydrogen bonding network since the corresponding residue of Ser-177 in LIP is an alanine in CcP.

The heme molecule is not planar but rather has a saddle-like shape with two pyrroles diagonal to each other being tilted toward the distal side and the other two pyrrole rings toward the proximal side of the heme. A least-squares plane calculated through the four nitrogen atoms of the pyrrole rings shows a almost perfect plane (r.m.s. deviation 0.03 Å) with the iron being in this plane (r.m.s. deviation 0.07 Å). The mean distance of the iron ion to the four pyrrole nitrogens is 2.02 Å. The overall geometry of the heme in ligninase compares very well with the heme in cytochrome *c* peroxidase [16]. Nonplanarity of the heme molecule is also observed in other heme proteins as for example in CcP and oxidized tuna cytochrome *c* [28]. It allows expansion of the inner core of the pyrrole nitrogens to suit high-spin ferric iron [29].

On the distal side of the heme close to the iron atom a water molecule has been assigned to a piece of spherical electron density. The Fe–O distance is roughtly 2.4 Å which is the same as found for the distal ligand in CcP [16]. The water molecule is connected to further discrete density extending roughly parallel to the propionate groups of the heme, approaching the entrance of the active site channel and extending further into the solvent region. This density is partially rather bulky. The shape and extent of the bulky portions of this density support the idea that it belongs to sugar molecules. The exact character of the sugar residues is not yet determined. Tentatively two mannose residues, as representatives of possible alternative pyranose saccharides, have been built into portions of the density (Fig. 6). Favouring hydrogen-bonding distances are found of the sugar hydroxyl groups with carbonyl atoms of adjacent amino acids. This supports furthermore the placement of sugar residues. The sugar molecules are in the neighbourhood of the C-terminal peptide with its potential *O*-glycosylation sites but on the opposite side of the enzyme with respect to the *N*-glycosylation site (Fig. 2). It is therefore likely that this polysaccharide chain originates from an *O*-glycosylation site.

As expected, the overall structure of ligninase shows some similarity to CcP. This correlates well with their principally equivalent chemical function. On the other hand noticeable differences are found especially for the ligation of the proximal histidine with the heme. The proximal histidine in CcP forms a hydrogen bond with a buried aspartic acid side chain [16]. It was proposed that this bond in CcP stabilizes high-oxidation states of the heme during catalysis. In LIP an equivalent bond with Asp-238 is formed. Here the distance is 3.02 Å which is practically the same as in CcP (2.93 Å). Therefore Asp-238 seems not to be the reason for the more positive redox potential [30] of lignin peroxidases and their ability to oxidize compounds of higher redox potentials. It is more likely that the weaker ligation of the heme iron with the proximal histidine in LIP415 causes the heme being more electron deficient than in CcP.

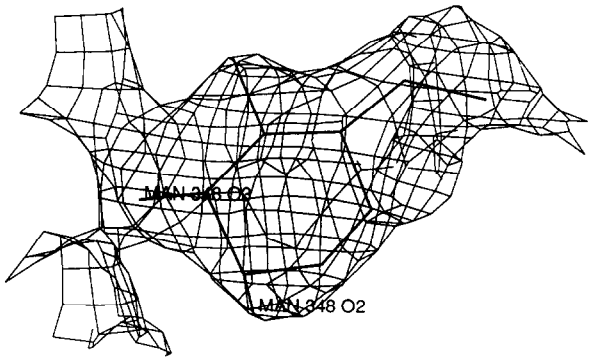

Fig. 6. One mannose (MAN) molecule at the active site entrance in its electron density (($|F_o| - F_c| \alpha_c$)). The hydroxylgroups O2 and O3 form hydrogen bonds with carbonyl atoms of the protein. Phases from the mannose were omitted to calculate the map.

Therefore it could be proposed that the ability of ligninase to oxidize compounds of high redox potential is related to the movement of the proximal histidine-containing helix caused by a strong hydrogen bonding network of Ser-177 to Asp-201 in an adjacent helix.

The coordinates of lignin peroxidase will be deposited with the Brookhaven Data Base on completion of the refinement. The current atomic positions are available from the corresponding author on request.

Acknowledgements: T.G. and K.P. are equal first authors. We thank the EMBL-Heidelberg/Germany for the opportunity to use their area detector. The authors would like to recognize the assistance of Dr. Paul Tucker (EMBL-Heidelberg) during data collection and processing. Gerko Hester is thanked for helpful discussions on the application of numerous computer programs and Thomas Choinowski for assistance in the preparation of the manuscript. This work was supported by the Academy of Finland (to T.G.) and the Swiss Institute of Technology Zürich (Grant 0-20-416-91 to T.G. and K.P.).

REFERENCES

[1] Adler, E. (1977) Wood Sci. Technol. 11, 169–218.
[2] Keyser, P., Kirk, T.K. and Zeikus, J.G. (1978) J. Bacteriol. 135, 790–797.
[3] Leisola, M.S.A., Kozulic, B., Meussdoerffer, F. and Fiechter, A. (1987) J. Biol. Chem. 262, 419–424.
[4] Glumoff, T., Harvey, P.J., Molinari, S., Goble, M., Frank, G., Palmer, J.M., Smit, J.D.G. and Leisola, M.S.A. (1990) Eur. J. Biochem. 187, 515–520.
[5] Sarkanen, S., Razal, R.A., Piccariello, T., Yamamoto, E. and Lewis, N.G. (1991) J. Biol. Chem. 266, 3636–3643.
[6] Tien, M. (1987) Crit. Rev. Microbiol. 15, 141–168.
[7] Eichhorn, G.L. and Marzilli, Eds. (1988) in: Advances in Inorganic Biochemistry, vol. 7, Elsevier, New York, Amsterdam, London.
[8] Schoemaker, H.E. (1990) Recl. Trav. Chim. Pays-Bas 109, 255–272.
[9] Valli, K. and Gold, M.H. (1991) J. Bacteriol. 173, 345–352.
[10] Glumoff, T., Winterhalter, K.H. and Smit, J.D.G. (1989) FEBS Lett. 257, 59–62.
[11] Dunford, H.B. and Stillman, J.S. (1976) Coord. Chem. Rev. 19, 187–251.
[12] McPherson, A. (1982) in: Preparation and Analysis of Protein Crystals, Wiley, New York.
[13] Thaller, C., Eichele, G., Weaver, L.H., Wilson, E., Karlsson, R. and Jansonius, J.N. (1985) Methods Enzymol. 114, 132–135.
[14] Matthews, B.W. (1968) J. Mol. Biol. 33, 491–497.
[15] Kabsch, W. (1988) J. Appl. Crystallogr. 21, 67–71.
[16] Finzel, B.C., Poulos, T.L. and Kraut, J. (1984) J. Biol. Chem. 259, 13027–13036.
[17] Crowther, R.A. (1972) in: The Molecular Replacement Method (M.G. Rossmann, Ed.), Gordon and Breach, New York.
[18] Fitzgerald, P.M.D. (1988) J. Appl. Crystallogr. 21, 273–278.
[19] Rossmann, M.G. and Blow, D.M. (1962) Acta Cryst. 15, 24–31.
[20] Wang, B.C. (1985) Methods Enzymol. 115, 90–112.
[21] Jones, T.A. (1978) J. Appl. Crystallogr. 11, 268–272.
[22] Jones, T.A., Zou, J.Y., Cowan, S.W. and Kjeldgaard, M. (1991) Acta Crystallogr. A47, 110–119.
[23] Brünger, A.T., Kuriyan, J. and Karplus, M. (1987) Science 235, 458–460.
[24] Hendrickson, W.A. and Konnert, J.H. (1981) in: Biomolecular Structure, Conformation, Function, and Evolution (R. Srinivasan, Ed.), Pergamon Press, Oxford, vol. 1, pp. 43–57.
[25] Ritch Jr., T.G., Nipper, V.J., Akileswaran, L., Smith, A.J., Pribnow, D.G. and Gold, M.H. (1991) Gene 107, 119–126.
[26] Schmidt, B., Heimgartner, U., Kozulic, B. and Leisola, M.S.A. (1990) J. Biotechnol. 13, 223–228.
[27] Hoard, J.L. (1971) Science 174, 1295–1302.
[28] Takano, T. and Dickerson, R.E. (1981) J. Mol. Biol. 153, 79–94.
[29] Scheidt, W.R. and Reed, C.A. (1981) Chem. Rev. 81, 543–555.
[30] Millis, C.D., Cai, D., Stankovich, M.T. and Tien, M. (1989) Biochemistry 28, 8484–8489.
[31] Kraulis, P.J. (1991) J. Appl. Crystallogr. 24, 946–950.